

Central Lancashire Online Knowledge (CLoK)

Title	Experimental and numerical analysis of microfluids Y-micromixer fabrication using CO2 laser
Type	Article
URL	https://clok.uclan.ac.uk/id/eprint/52102/
DOI	https://doi.org/10.1007/s11082-024-07135-7
Date	2024
Citation	Salman, Safa N., Rajab, Fatema H., Issa, Ahmed and Al Shaer, Ahmad Wael (2024) Experimental and numerical analysis of microfluids Y-micromixer fabrication using CO2 laser. Optical and Quantum Electronics, 56 (7). ISSN 0306-8919
Creators	Salman, Safa N., Rajab, Fatema H., Issa, Ahmed and Al Shaer, Ahmad Wael

It is advisable to refer to the publisher's version if you intend to cite from the work. https://doi.org/10.1007/s11082-024-07135-7

For information about Research at UCLan please go to http://www.uclan.ac.uk/research/

All outputs in CLoK are protected by Intellectual Property Rights law, including Copyright law. Copyright, IPR and Moral Rights for the works on this site are retained by the individual authors and/or other copyright owners. Terms and conditions for use of this material are defined in the http://clok.uclan.ac.uk/policies/

Experimental and Numerical Analysis of Microfluids Y-Micromixer Fabrication Using CO₂ Laser

Safa N. Salman¹, Fatema H. Rajab*¹, Ahmad Issa² and Ahmad W. Alshaer³

Corresponding author: E-mail: fatema.h.rajab@nahrainuniv.edu.iq, fatema.hamid.rajab@gmail.com, fatemarajab83@gmail.com

Abstract

Microfluidic devices (MFD) have several applications in the chemical and biomedical analysis field such as mixing two different drugs prescribed to inpatients. Micromixer can be fabricated using laser beam to ablate microchannel on the surface of polymeric substrate.

In this work, CO₂ laser was used to manufacture MFD on polymethyl methacrylate (PMMA) substrate with straight and zigzag profiles by investigating the effect of processing parameters (scanning speed, laser power and depth of focus) on the ablated microchannel width, depth, aspect ratio and wettability. The focus is to produce channel with depths from around 50µm to 1600µm using one system, hence producing large microchannels which were not studied in most of the report work. Then a CFD model was developed to characterize the effect of channel geometry and liquid diffusivity and speed on the fluids mixing efficiency.

The results showed that the crater width, depth, aspect ratio (AR), surface hydrophilicity and surface temperature increased with increasing laser fluence, and the effect of the process dynamics at constant fluences was also investigated. Various channel profiles such as V-shaped and U-shaped cross sections were produced by shifting the focal position of the beam. This is important in the design phase of the channels, since our single pass method of machining offers a full range of AR from around 0.3 up to 2.25, and a channel depth of $47\mu\text{m}$ -1600 μm . The results also showed that the mixing efficiency significantly relies on the channel geometry and fluid flow characteristics, with a maximum mixing efficiency of 99.9% was recorded using a squared shaped MFD.

Keywords: Micromixer, MFD, PMMA, Microchannel, CO₂ laser, COMSOL, Mixing efficiency

Table of Nomenclature	Rajab and Al-Hamd 2023: Vora et	al 2013)
1 a o i c o i romenciala e	Kajao anu Ai-mainu 2023. Voia Ci	a 1. 2013 1.

Abbreviation	Description
ρ	Density (in kilograms per cubic meter)
c_p	Specific heat at constant pressure (in joules per kilogram per kelvin)
k	Thermal conductivity (in watts per meter per kelvin)
T	Temperature (in kelvin)
t	Time (in seconds)
x	x-coordinate
у	y-coordinate
Z	z-coordinate
P	Laser power density

¹ Department of Laser and Optoelectronics Engineering, College of Engineering, Al-Nahrain University, Jadyria, Baghdad, Iraq, 1007

² Mechatronics and Medical Devices Engineering Department, Faculty of Engineering and Information Technology, Al Azhar University-Gaza, Palestine

³School of Engineering, University of Central Lancashire, Preston, UK.

h	Heat transfer coefficient
T_a	Ambient temperature
A	Absorptivity
V	Scanning speed
t	Time
ε	Emissivity
σ	Stefan-Boltzmann constant

1. Introduction

Microfluidics is a field that studies the control of very small fluids ranging in size from microliters (μL) to picolitres (pL). This field offers important benefits such as heat transfer and low volume requirements for reagents and samples. It also provides high signals compared to the noise ratio when the image is detected (Vannoy et al. 2011). Miniaturization also gives integration of parallel structures in one device to produce high analysis within a short time. In the past decade, this field has found wide interest for its use in applications related to medical diagnosis and clinical analysis, environmental pharmacokinetics, genetics, forensic medicine and proteomics (Verpoorte 2002).

Different materials have been used to manufacture these devices depending on the application. Recently, glass, silicone and polymer have been used to manufacture microfluidic devices (Aralekallu et al. 2022). Because silicon is opaque to visible wavelengths of light, its uses in manufacturing microfluidic devices (MFD) are limited. It is not suitable for high voltage applied to capillary electrophoresis and pumping electrophoresis used in special applications in the field of microfluidics(Abgrall and Gue 2007). One of the most used detection techniques is optical detection, as it was used in the science of separation and transparency of microfluidic devices. Polymers have many advantages over silicone and glass including good chemical resistance, biocompatibility, low cost, optical properties and the ability to be mass produced using currently used manufacturing techniques such as injection moulding and hot embossing(Roy et al. 2011). In thermoplastics, polymers are used in manufacturing on a large scale, and the most widely used plastics are PMMA and PC(Becker and Gärtner 2008).

Based on their geometry, MFDs are available with different designs such as straight channel, Y- channel, T-junction, cross-junction, spiral, and X- channel. In the field of microfluidics, photolithography, etching, soft lithograpy, precision micromachining (micro milling), hot embossing, injection moulding, and laser ablation are the most frequently used methods for creating microchannel and other microfeatures (Becker and Gärtner 2008; Iliescu et al. 2012; Verpoorte and De Rooij 2003; McDonald et al.

2000; Becker and Locascio 2002; Heckele et al. 1998; Lippert 2004). Laser processing is comparable because it offers a precise, rapid, and non-contact option to traditional methods, with the added benefit of flexibility in terms of the materials, designs, and features that can be created. Its user-friendly operation makes it an ideal tool for quickly prototyping both simple and complex designs. Furthermore, laser processing can be utilized to integrate complementary functions into microfluidic devices, such as creating patterns of microelectrodes within thin metal films located inside microchannels (Khan Malek 2006).

Different lasers have been used for manufacturing MFD such as CO2, diode and ultrashort lasers. The selection of lasers and processing parameters depends on the used materials and the desired properties of MFD, and each laser has positive and negative effects. Using CO₂ laser, there are several published works focused on analyzing the effect of processing parameters on channel characteristics(Gucluer and Guler 2023; Malek 2006). Ting-Fu Hong et al. studied the rapid prototyping of PMMA microfluidic chips utilizing a CO₂ laser (Ting-Fu Hong et al. 2010). Yiqiang Fan et al. studied the effect of using a novel technique of CO₂ laser machining of wax-covered plastic paper on microchannel quality (Yiqiang Fan Huawei Li Ying Yi Ian G. Foulds 2013). S. Prakash and S. Kumar fabricated a microchannel on PMMA using a CO₂ laser for microfluidic applications. They studied the effect of laser power and scanning speed on the width, depth, and softened zone of microchannel, and, on another study, they created a microchannel with rectangular cross-sections on PMMA using a CO₂ laser in combination with an underwater-fabricated 40 µm thick copper mask using a Fiber laser (Prakash and Kumar 2015; Prakash and Kumar 2017). J. Cai et al. produced a MFD utilizing a 10.6 µm, CO₂ laser on COC polymer. The ablated microchannel exhibited a Gaussian-like profile. Variations in the width and depth of the microchannels were observed under different laser power and scan speeds and the smallest achievable width and depth for the microchannels are approximately 223 µm and 132 µm respectively (Cai et al. 2017). Carlos Matellan et al. analyzed the effect of laser power and focus point on microchannel width and depth and studied the cost-effective rapid prototyping and assembly of PMMA microfluidic devices using CO₂ laser. Here, the residues were eliminated using isopropyl alcohol (Matellan and del Río Hernández 2018). Yundong Ren et al. manufactured and developed the reconfigurable acrylic-tape hybrid microfluidics which is useful in the medical and clinical fields using a direct and quick manufacturing method with CO₂ laser (Yundong Ren et al. 2019). Mahdee Samae et al. manufactured paper-based Y-shaped micromixer with straight and zigzag (Mahdee Samae · Pawarit Ritmetee · Somyot Chirasatitsin · Sanja Kojić · Tijana Kojić · Jovana Jevremov · Goran Stojanović · Hani Al Salami 2019). Sanja P. Kojic et al. manufactured a Y-shaped with a straight and zigzag design on a Ceram Tape layer between two PVC foils layers using xerography technique and laser micromachining process (Sanja P. Kojic 2019). S. Gucluer and O. Guler proposed a simple, rapid MFD fabrication method for separating cells and bacteria-size microparticles using CO₂ laser (Gucluer and Guler 2023). Diode laser, on the other hand, have been also used for manufacturing MFD and it has been proved that V-shaped microchannel could be formed using diode laser while a U-shaped channel is formed using CO₂ laser (Kexin Gao et al. 2019). Ultra-short lasers (ps and fs) have also been used for MFD manufacturing on glass substrate where the laser processing was followed by chemical treatment using KOH and HF for enhancing the performance of microchannel (LoTurco et al. 2013; (Sungil Kim 2018; Wlodarczyk et al. 2019).

Numerically, several works have been conducted to analyze the MFD performance. A. Farahinia et al. analyzed and investigated the impact of different cross-sections and input angles on the mixing performance of microfluidic mixer numerically using COMSOL software. Two types of channel cross-sections were examined: circular and rectangular. A. Bonament et al. proposed a 2D analytical model for the prediction of the concentration profiles at the outlet of a passive mixer. They studied the effect of shape (Y and line) and the length of the channel (Bonament et al. 2022; Farahinia and Zhang 2020).

To the best of our knowledge, there are limited published works that focused on reporting an experimental analysis for selecting appropriate laser processing parameters for MFD fabrication efficiently. Most previous research work were either limited to manufacturing "small" channels with dimensions less than 500μm or developing analytical or numerical models with limited validation of fluid delivery or the channels dimensions. Therefore, the focus of this work is to perform a comprehensive experimental analysis using CO₂ laser micromachining system to produce channel with depths from around 50μm to 1600μm using one system. This is accompanied with the development of a 3D thermal model to simulate the effect of processing parameters on the surface temperature and craters' ablation characteristics. Furthermore, a 2D CFD model is adopted to analyze and validate the performance of a Y-channel MFD simulated using FEA (COMSOL Software).

2. Material and Method

2.1. Microchannel Fabrication

A transparent PMMA workpiece with a dimension of (20×10×2) mm is selected in this work. The physical properties of PMMA is listed in table1. The CO₂ laser beam was used for the generation of microchannels. CA-1500 CO₂ laser from PI MICOS is a CW laser with a wavelength of 10.6 μm. Its maximum power is 100 W. This laser is delivered with a full working software with control computer with all necessary drives including control software. The laser is delivered also with a workstation including x-y stages. The software package consists of the main control program for the CA-1500 kit to control the full working of the laser. For example, it is used to control the x-y stages movements. A software such as AutoCAD and CAD converter were used in this project. Table 2 listed the used processing parameters for microchannel fabrication.

Table 1: Physical properties of PMMA (Li et al. 2018).

Property	PMMA
Young's Modulus (GPa)	2.4
Poisson ratio	0.37
Density (kg/m ³)	1185
Thermal conductivity (W/m ² . K)	0.2
Specific heat (J/kg. K)	1466
Thermal expansion (K-1)	4.4×10^{-4}
Glass transition temperature (°C)	105
Melting temperature (°C)	220

Table 2: Laser processing parameters.

Power [W]	5 ,10 ,15 ,20 ,30
Focal Position (distance from the focal point) [mm]	-10, -5, 0, +5, +10
Scanning Speed [mm/s]	2, 4, 6
Spot size [mm]	0.5

The PMMA machining occurred using a sheet supplied by credible supplier, and was stored for very short time in a room temperature around 20 °C and in a lab with humidity of less than 10%. Therefore, those conditions will endure that PMMA holds its thermomechanical properties and does not change before processing. Moreover, the experiments were conducted within hours of receiving the samples, hence not allowing for long-time storage that may affect the materials properties.

2.2. MFD Fabrication

The proposed MFD consists of two layers, as shown in Figure 1. Top layer was realized using PMMA adhesive layer. The down layer was used for fabrication of different MFD structures. Firstly, the simple Y-channel was fabricated using different Y angle of incident to select the best angle for fabricating the other designs. Multiples laser passes

was used to get rid of residuals and blockage in the Y intersect area. The best angle (90°) was selected, due to its best mixing efficiency, and used for fabrication of all MFD structures (straight, zigzag with 45°, zigzag with 90°, zigzag with curved edges). The 20 W laser power, -10 mm focus position, 6 mm/s scanning speed, 5 times processing was used for MFD manufacturing. For hole creation on top layer (5 W power, 1pass, 0.5 mm spot size) processing parameters were used.

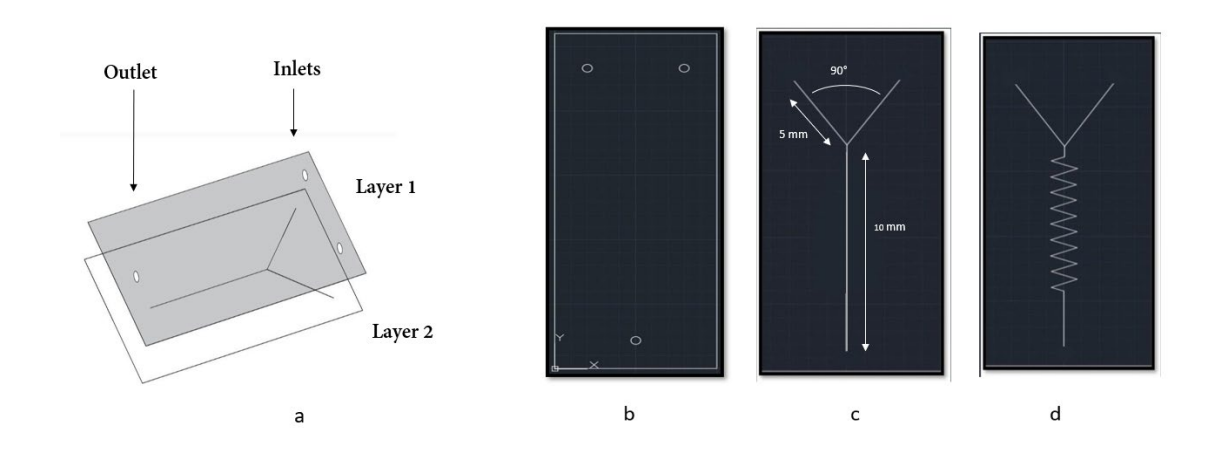


Figure 1: (a) model of MFD, (b) top layer, (c) simply straight Y channel, and (d) zigzag channel.

2.3. Microchannel and MFD Characterization

Optical microscope (Model: ALTAY) has been used to analyze the surface morphology. The images of the laser treated surfaces was analyzed using 5X magnification. The images were taken using a high-resolution digital camera from the eyepiece and analyzed using ImageJ software. For wettability characterization, a sessile drop method was used(Rajab et al. 2021b). Here, a 50µL drop of water was placed on the surface, and an image was captured using a microscope (see Figure 5s). Next, image J software was used to measure the contact angle from left and right and the average contact angle was recorded. This method has been used to measure the contact angle and investigate the impact of laser parameters on the wettability of the surface. The wettability was characterized to understand the effect of laser parameters on the channel's profile, which in turn affects the quality of the bonding process.

3. Computational Modeling

3.1. Thermal Modeling of Microchannel

In this study, a Model of continuous, CO₂ laser thermal heating of PMMA in air was built using 6.0 COMSOL Multiphysics. A 3D geometry (Figure 2) and a time-

dependent study are considered. The length and width of the geometry are 10 mm and 6 mm, respectively while the thickness is 2mm. The elements with T>T_m are excluded from geometry (where T and T_m are surface and melting temperatures respectively). The modelling was considered using a 10.6 μ m laser wavelength. Figure 3 shows the flow diagram of the modelling approach. The heat source, heat convection and surface to ambient radiation is considered on the upper boundary (boundary 1). Extremely fine with 200 μ m and 2 μ m maximum and minimum element size, respectively, was applied on the upper boundary (boundary 1), while free tetrahedral with 4 iterations was applied on the remaining geometry. The number of elements was 23750 (see Figure 1s in the appendix). Tables 3 lists the governing equations and boundary conditions of heat transfer mode, respectively.

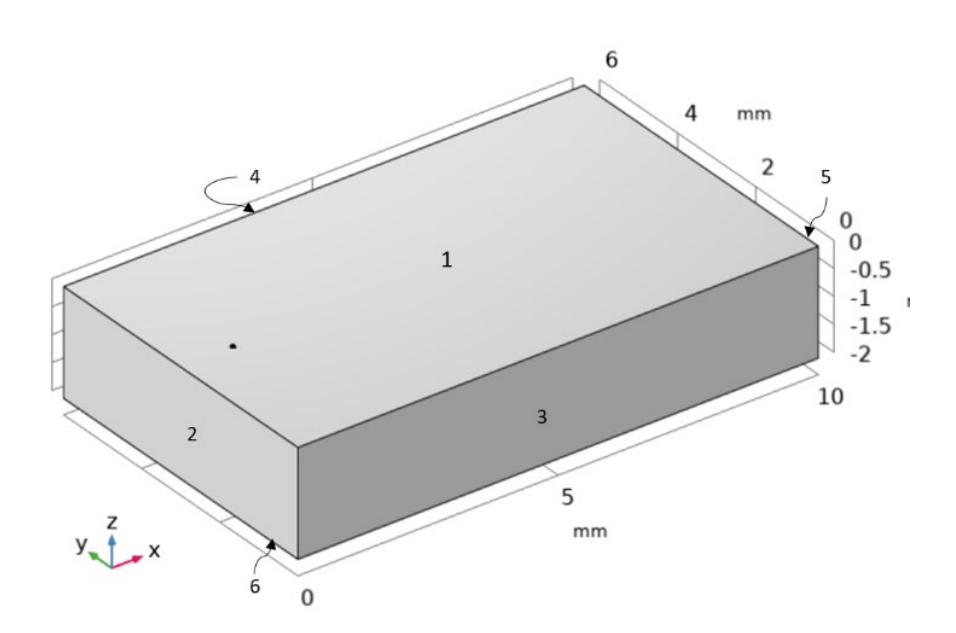


Figure 2: Geometry using the modeling.

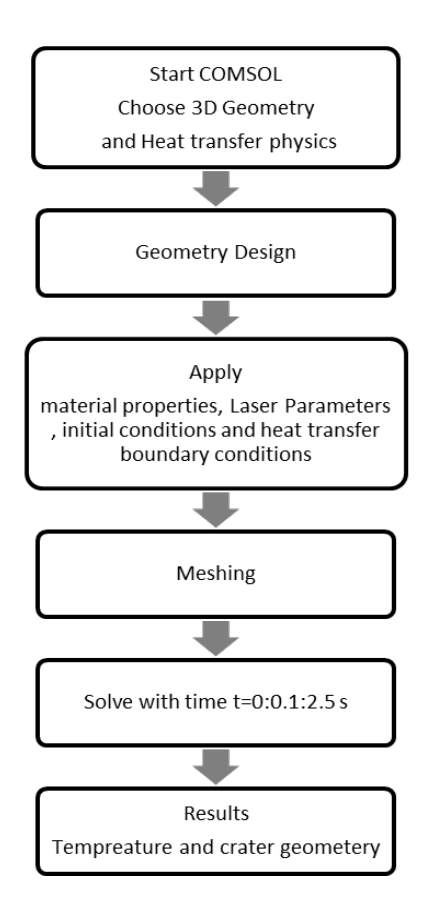


Figure 3: The flow diagram of the modelling approach.

Table 3: Governing equations and boundary conditions of heat transfer model (Rajab and Al-Hamd 2023; Vora et al. 2013).

Boundary no.	Boundary condition	Equation
Whole geometry	Governing equation	$\rho c_p \left[\frac{\partial T}{\partial t} \right] = k \left[\left(\frac{\partial^2 T}{\partial x^2} \right) + \left(\frac{\partial^2 T}{\partial y^2} \right) + \left(\frac{\partial^2 T}{\partial z^2} \right) \right]$
1	Heat flux, natural convection cooling and radiation	$-k\frac{\partial T}{\partial y} = P - h[T - T_a] - \varepsilon\sigma[T^4 - T_a^4]$
	Laser power density in Gaussian distribution	$P = A \left[\frac{P}{(\pi r_{spot}^{2})} \right] exp \left[-\frac{2r_{focus}^{2}}{r_{spot}^{2}} \right]$
		$r_{focus} = \sqrt{x_{focus}^2 + y_{focus}^2}$
		$x_{focus} = x_0 + Vt$ $y_{focus} = y_0$
1	Natural convection cooling and radiation	$egin{align} -krac{\partial T}{\partial y} &= h[T-T_a] - arepsilon\sigma[T^4-T_a^4] \ -krac{\partial T}{\partial x} &= h[T-T_a] - arepsilon\sigma[T^4-T_a^4] \ \end{matrix}$
2,3,4,5,6	Insulation	$\frac{\partial x}{\partial y} = 0$

3.2 Computational Fluid Dynamic Modeling

Here, COMSOL 6.0 was also used to design 2D Y-channel MFD and analyze the effect of angle of incident, channel width and length, inlet length, and diffusion coefficient on mixing concertation and efficiency. Y-shaped micromixer is displayed in Figure 4 and

its dimension listed in Table 4. Each inlet has 5 mm length and 250 µm width. The results of straight micromixer are compared with squared Y-micromixer.

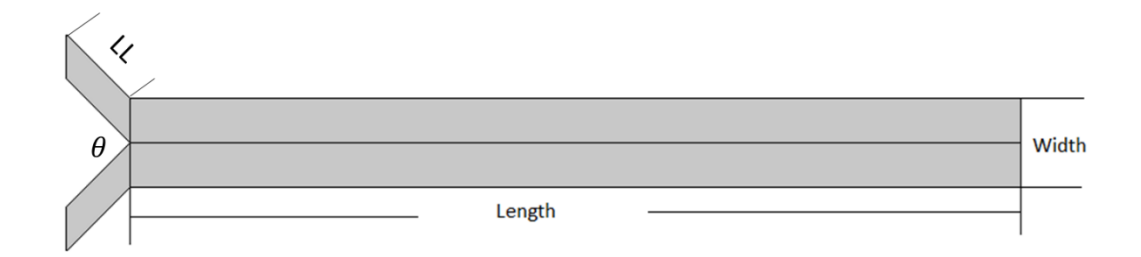


Figure 4: Y-shaped micromixer.

Table 4: Parameters of Y-micromixer.

θ	90° ,60° ,30°
Length	10-40 mm
Width	0.1-0.5 mm
LL	1-5 mm
shape	Y strait and square
Concentration of liquid in both channel	10 μΜ
Input velocity	1 cm/s

Two flows with concentration value (c0,1=1 mol/m³) are imposed to both entrances leading to similar distribution of the velocity along the channel. The velocity and pressure at flow inlet and outlet are equal to 1 cm/s and zero, respectively. The mixing occurs mainly with the main channel of micromixer having 0.5 mm width and 10 mm length. Figure 5 presents the flowchart of modeling approach. Grid convergence index was handled, then finer physics-controlled mesh sequence type with about 19688 elements and 0.8003 average element quality was conducted (see Figure 2s in the appendix). Time-dependent with 0.01 time step, 0.5 absolute tolerance factor, BDF time stepping, 2 BDF maximum order and 8 maximum number of iterations was used.

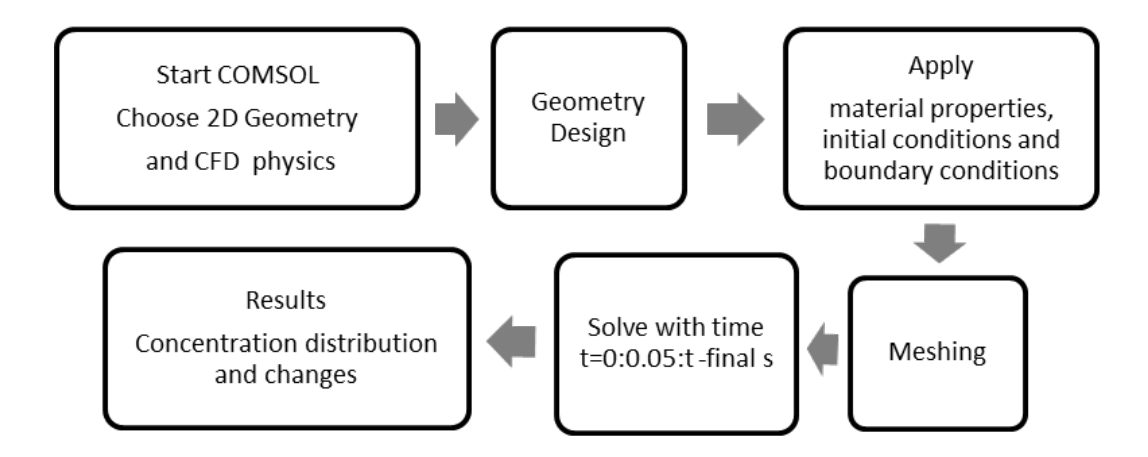


Figure 5: Flow diagram of modelling approach.

Diffusion is a critical factor in the mixing phenomenon, representing an essential physical process based on the concept of Brownian motion. Brownian motion describes how particles from regions of higher concentration in the fluid move towards regions of lower concentration, gradually contributing to the mixing of substances. Fick's law, which describes the used diffusion in this work, is defined by the following equation (Conlisk 2012; Farahinia and Zhang 2020).

$$j=-D (dc/dx)$$
 (1)

where c, x and D are the reagent's concentration (mol/m³), the species' position within the microchannel (mm), and the diffusion constant (m²/s), respectively. Equations 2 and 3, which are the Navier–Stokes equation and the Continuity equation, are typically used to characterize the motion of an incompressible Newtonian fluid in microchannel (Baccar et al. 2009).

$$\rho \frac{\partial V}{\partial t} + \rho(V.\nabla)V - \eta \nabla V + \nabla P = 0$$

$$\nabla . V = 0$$
(2)

Where V, P, η and ρ denote the velocity, signifies pressure, dynamic viscosity, and fluid density, respectively.

When exiting the microchannel, the inlet velocity boundary condition is applied as the driving force to the inputs. In such situations, the pressure boundary condition is set to zero. Additionally, it is assumed that all microchannel walls exhibit a non-slip boundary condition. In Equation 4, referred to as the Reynolds number, the symbols U, L, and μ correspond to the fluid velocity, microchannel length, and dynamic viscosity,

respectively. This dimensionless number, which quantifies the balance between inertial and viscous forces, provides insight into whether the flow is laminar or turbulent. For instance, a lower Reynolds number indicates a predominance of laminar flow due to the damping effect of viscous forces on disturbances.

$$Re = \frac{\rho UL}{\mu} \tag{4}$$

The particle transport within an incompressible flow is described by Equation 5

$$\frac{\partial c}{\partial t} + V \cdot \nabla C = \nabla \cdot (D\nabla C) + R \tag{5}$$

where *R* signifies the rate of concentration change due to chemical reactions which be set to zero in this simulation since no chemical reactions occur. Subsequently, the Navier–Stokes equations need to be solved separately under the specified conditions to obtain the velocity field. Consequently, the obtained solution is then applied to address the steady-state convection–diffusion equation. Then Equation (6) was used for mixing efficiency calculation (Chen et al. 2006)

$$\sigma = \left[1 - \frac{\sqrt{\frac{1}{N} \sum_{1}^{N} (c - c_{\infty})^{2}}}{\sqrt{\frac{1}{N} \sum_{1}^{N} (c_{0} - c_{\infty})^{2}}}\right] \times 100\%$$
 (6)

Where c_0 , c_∞ , and N are, respectively, the initial concentration (two fluids are not combined), concentration with comprehensive mixing, and number of nodes.

4. Results and Discussion

4.1. Micromachining of PMMA

Before implementing MFD, different parameters have been investigated to study their effects on microchannel fabrication on PMMA. The experiment involved manipulating different processing parameters (scanning speed, laser power and distance between the laser and the polymer sample (PMMA)) to analyze the effect of processing parameters on microchannel width, depth and morphology. Figure 6 shows the optical images using different processing parameters for single line machining. It can be seen from Figure 6a at the focal point of the laser beam (0 mm), a V-shape was observed, while U-shape or circular-shaped channel was observed using out-of-focus laser machining and at (+5 mm, +10 mm) exhibited a significantly large heat-affected area. Figure 6b shows the optical images of PMMA sample machined using different power, 4 mm/s scanning speed, and (+5 mm). The width and depth of the microchannel increased with laser

power and the higher aspect ratio was achieved at (30W), where the laser's impact on the sample displayed a distinctive y-shape. Figure 6c shows three optical images of PMMA using different scanning speeds (2mm/s, 4mm/s,6mm/s) t turns out that the best shape (U-shape) was obtained at speed 6mm/s. In contrast, lower energy settings produced a circular shape with greater width and shallower depth. The reaction time is a crucial factor that influences the size of the heat-affected zone, and this can be controlled through the laser's speed. Higher speed reduces the heat-affected zone, resulting in a clearer and more defined engraving shape on the sample (Prakash and Kumar 2016).

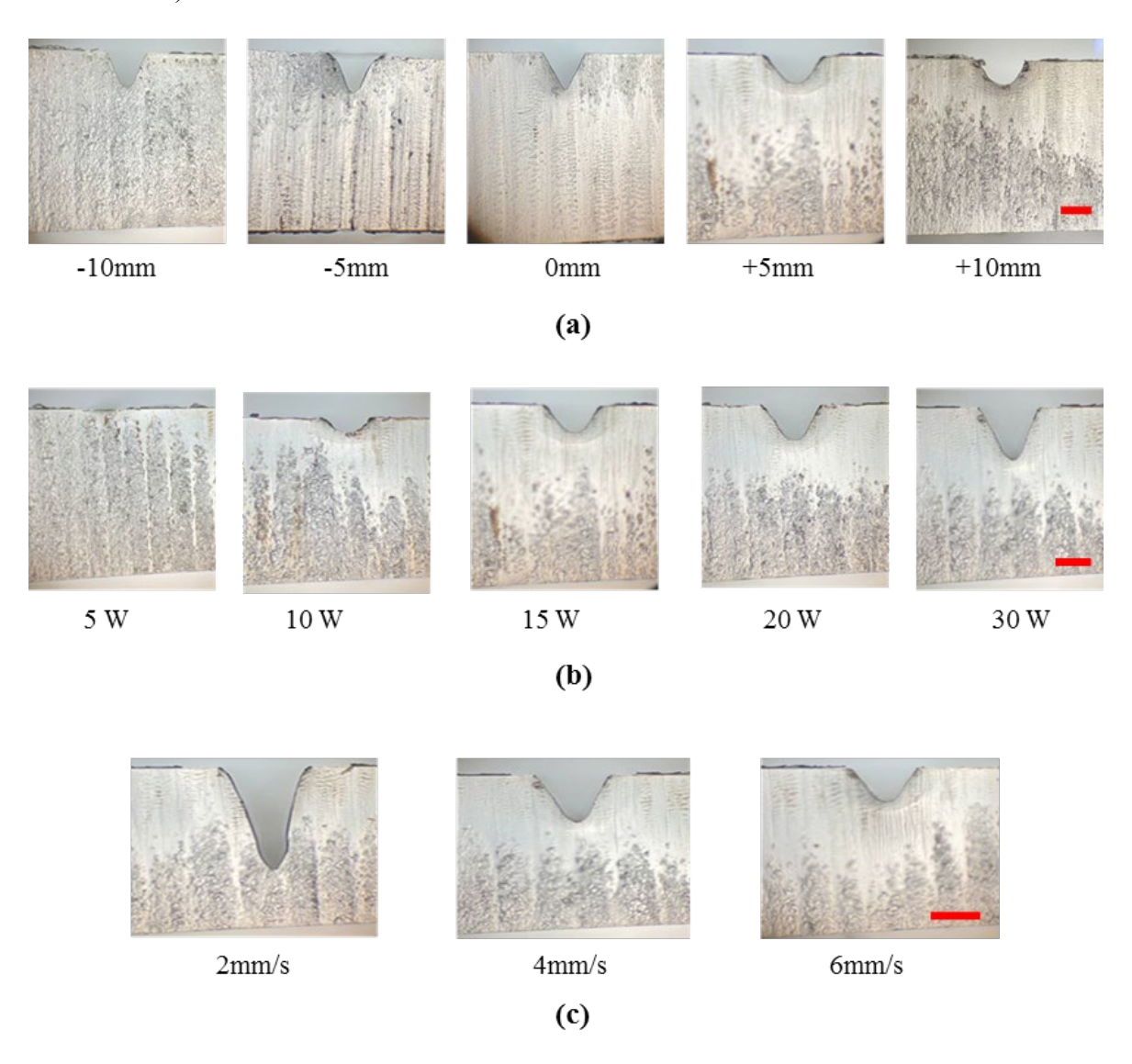


Figure 6: The crater morphology by changing different laser processing parameters: (a) focal position using 4mm/s and 15W, (b) beam power using 4mm/s and +5mm, and (c) scanning speed using 30W and +5mm respectively. The scale bar = 500μm.

Figure 7 and 8 illustrate the statistical analysis of how varying scanning speeds, different energy, and changes in focal position affect the depth and width of

microchannel respectively. Data for ± 10 mm focus position are inserted in the appendix to avoid graph repetition.

As expected, deeper microchannels were produced at focus and by increasing the laser power and decreasing the scanning speed, however, in a very sensitive fashion. For instance, increasing the power by 6 times, increased the depth by around 15 times, while increasing the travel speed by 3 times reduced the depth by more than 60%. This sensitivity is also noticed at various focal positions. Using the highest level of energy input (at 30W and 2mm/s), the maximum channel depth ranged between 900 µm to 1.58mm depending on the focal position, while a minimum channel depth of 53 µm was achieved at 5W and 6mm/s. It must be noted that focusing the 5W beam at ±10mm and+5mm did not achieve any machining and the energy was not adequate to raise the temperature above the vaporization point, however ablation could only be achieved at focus and 5mm below the surface (see Figure 3s in appendix). This can be explained by the plasma lensing effect which lifts the laser beam's focus position upwards due to the plasma plume, causing the focused beam at -5mm to shift upwards and allow for adequate laser intensity to ablate the polymer (Ravi-Kumar et al. 2019).

In Figure 8 (see Figure 4s in the appendix for ±10mm focus), a lot less sensitivity of the microchannel width to varying scanning speeds, laser power, and the focal position is noted. The results showed that a higher width was observed at +10mm focus position compared to the focused beam, which is related to the larger spot size, although this is usually accompanied with shallower channels. Larger spot size reduced the fluence and expose larger surface to convection and conduction to the surrounding, which results in shallower depth, but larger width. Using the highest level of energy input (at 30W and 2mm/s), the maximum channel width ranged between 0.7 mm to 0.9mm depending on the focal position, while this value minimum ranged 0.0-0.2 mm when the minimum heat input was used at 5W and 6mm/s (see also Figure 4s in appendix).

Figure 9 depicts the change in the microchannel's dimensions and aspect ratio with the line energy (calculated by dividing the power by the speed) and the volumetric laser fluence (calculated by dividing the line energy by the cross-sectional area of the machined crater). It is clear that the volumetric fluence decreases as the width and depth increases because this causes the cross section to increase. The aspect ratio curve follows the microchannel's depth and both quantities steadily increase by smaller intervals for fluences values more than 30 J/mm³, while the change significantly accelerate below 30 J/mm³. The microchannel's dimensions becomes equal at 27.3

J/mm³ with an aspect ratio of around "1", while the AR value reaches "2.25" at the fluence level of 26.1 J/mm³.

It is clear the channel's depth changed faster than the width as the fluence decreased and the line energy increased, hence increasing the AR accordingly. This can be related to the laser's Gaussian profile in which the power is concentrated at the center and fades out towards the circumference, hence increasing the power (when the spot size is fixed) will enhance the heat flux at the centre and increase the machining effect vertically. This corresponds to other researcher's (Prakash and Kumar 2021; Prakash and Kumar 2015) findings, although they suggest a linear relationship between power and machining depth. The relationship observed in Figure 9 is clearly not linear and covers a much larger range of fluence values. Moreover, it experimentally offer a more realistic view because the linear power-depth relationship neglects conduction, convection and other phenomena associated with laser beam movement, such as air flow dynamics, plasma effect etc, which may significantly affect machining results, especially at higher fluence values.

Figure 9 is important in the design phase of the channels, since our single pass method of machining offers a full range of AR from around 0.3 up to 2.25, and a depth range between $47\mu m$ to $1600\mu m$.

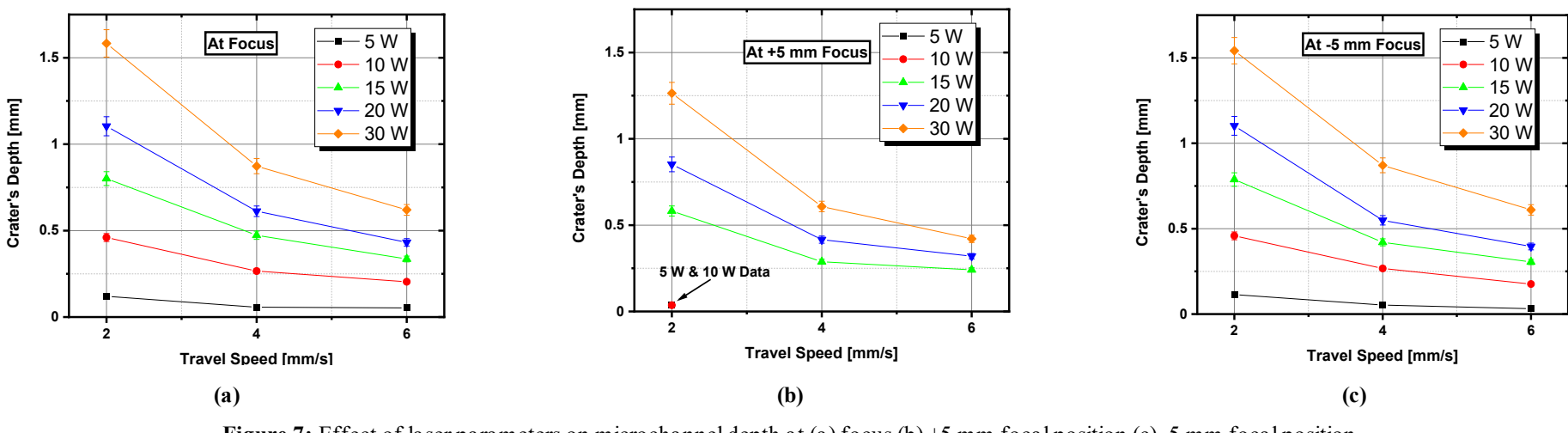


Figure 7: Effect of laser parameters on microchannel depth at (a) focus (b) +5 mm focal position (c) -5 mm focal position.

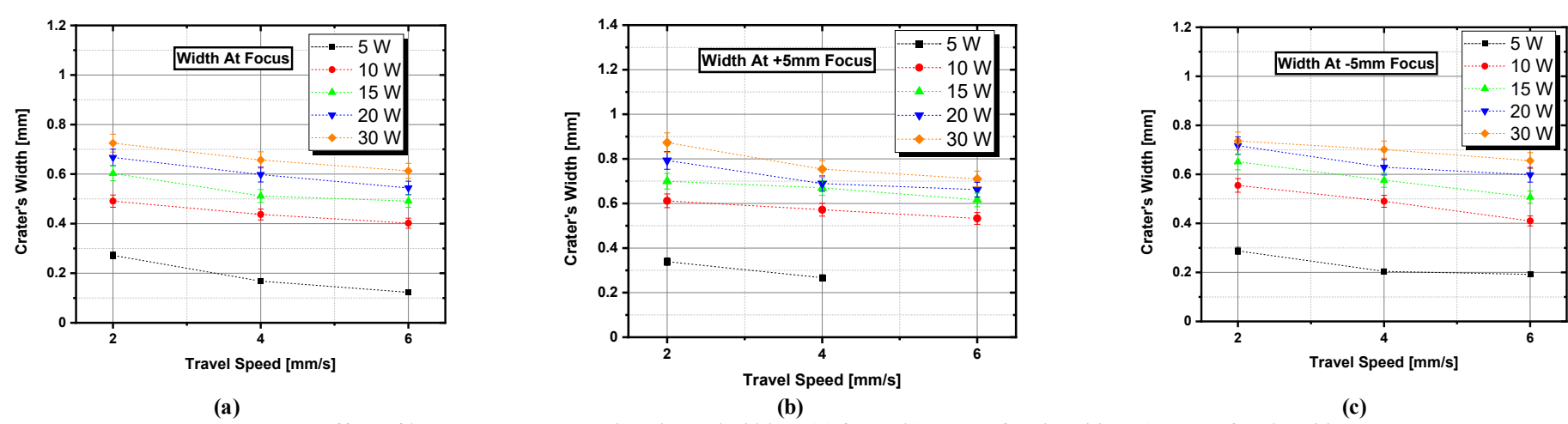


Figure 8: Effect of laser parameters on microchannel width at (a) focus (b) +5 mm focal position (c) -5 mm focal position.

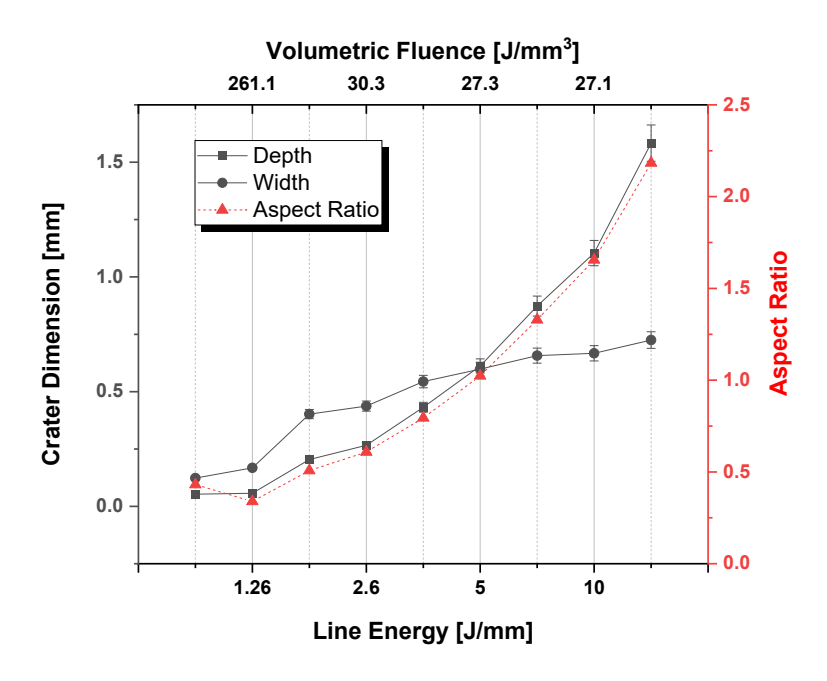


Figure 9: Effect of laser fluence/line energy on microchannel dimensions and aspect ratio at focus.

Figure 10 depicts the change in AR, depth and width by increasing laser power and speed, while maintaining a constant energy level although the same heat input is used in each of the sub-figures, the ablation dynamics and the material-laser interaction may be different, which is clear from Figure 10(a) that shows that simultaneous increase in speed and power would increase the microchannel dimensions by around 2.5 times and the AR by 1.5 times at a constant line energy of 2.5J/mm. This trend continues up to 5 J/mm (at 4mm/s and 10W), above which changing the speed and power does not have a significant effect on the channel's dimensions and aspect ratio.

Higher speeds reduce the interaction time between the laser and matter and would generally lead to shallower channels if the fluence was kept constant. In PMMA, however, the heat conduction wave seems to move faster as the power is increased despite the corresponding rise in the travel speed. This is evidenced using COMSOL simulation in Figure 12(a) which shows the temperature temporal change at the 2.5 J/mm (2mm/s, 5W and 4mm/s, 10W) and that the maximum temperature using 10W and 4mm/s (5300 K) is higher than that using 5W and 2mm/s (4400 K). This shows that at low line energy levels, the conduction wave front moves faster and ablates more material, producing larger crater. However, when the line energy reaches a threshold (5 J/mm or 12.7 J/mm³ for PMMA) the speed becomes irrelevant to changing the crater profile since the heat wave has already heated up a large volume of the material. This

indeed may be differed if higher speeds than 6mm/s were used, but testing larger range of speeds is out of the scope of this article.

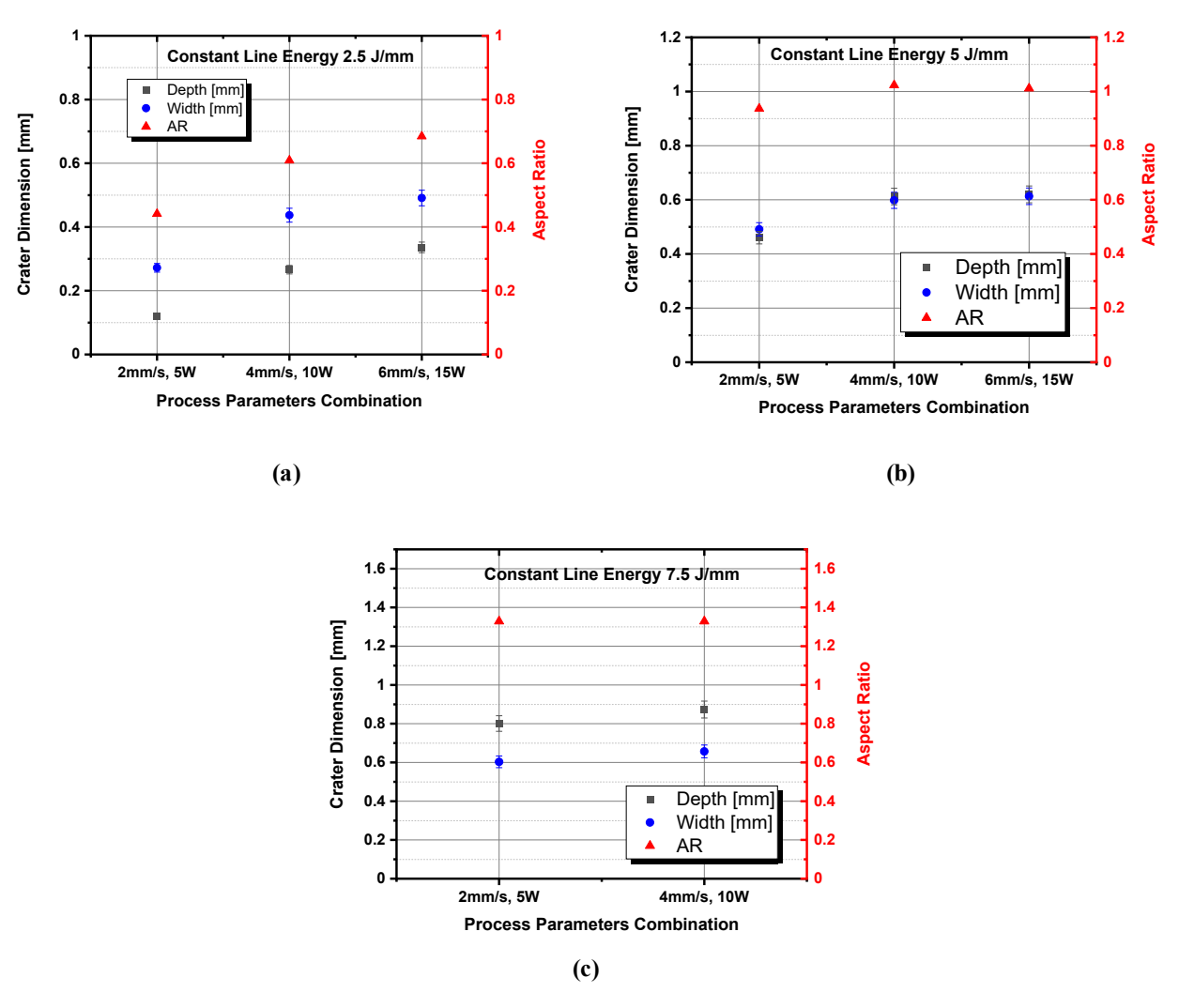


Figure 10: Effect of constant line energy (a)2.5 J/mm (b) 5 J/mm and (c) 7.5 J/mm on the microchannel's dimensions and AR at focus.

Figures 11a-c illustrate how the laser processing parameters affect the measurement of the contact angle of the droplet above the channel machined using different processing parameters (see Figure 5s). Figure (11a) shows the contact angle increases as the scanning speed increases, indicating that the hydrophobicity increases with increasing the scanning speed with minimum value of 47° using 2 mm/s. Since the contact angle's highest value reached 72° at 5W, and its lowest value 47°at 30W, when it came to power, it can be said that the hydrophilicity correlates directly to the laser power Figure (11b). The relationship between DOF (depth of focus) and contact angle is not clearly correlated, but it is evident in Figure (11c), where it reaches its maximum value at the focus where the angle value reaches 65°. We believe this is due to the V-shape and the fact that the microstructure of the surface, which produced the lowest contact angle and

highest hydrophilicity at -10 mm, where the contact angle reached 48°, influences wettability. It is evident that the laser processing parameters affects the microstructure of the target which in turn affected the wettability (Rajab et al. 2021a; Rajab et al. 2018; Rajab et al. 2017; Rajab and Al-Hamd 2023).

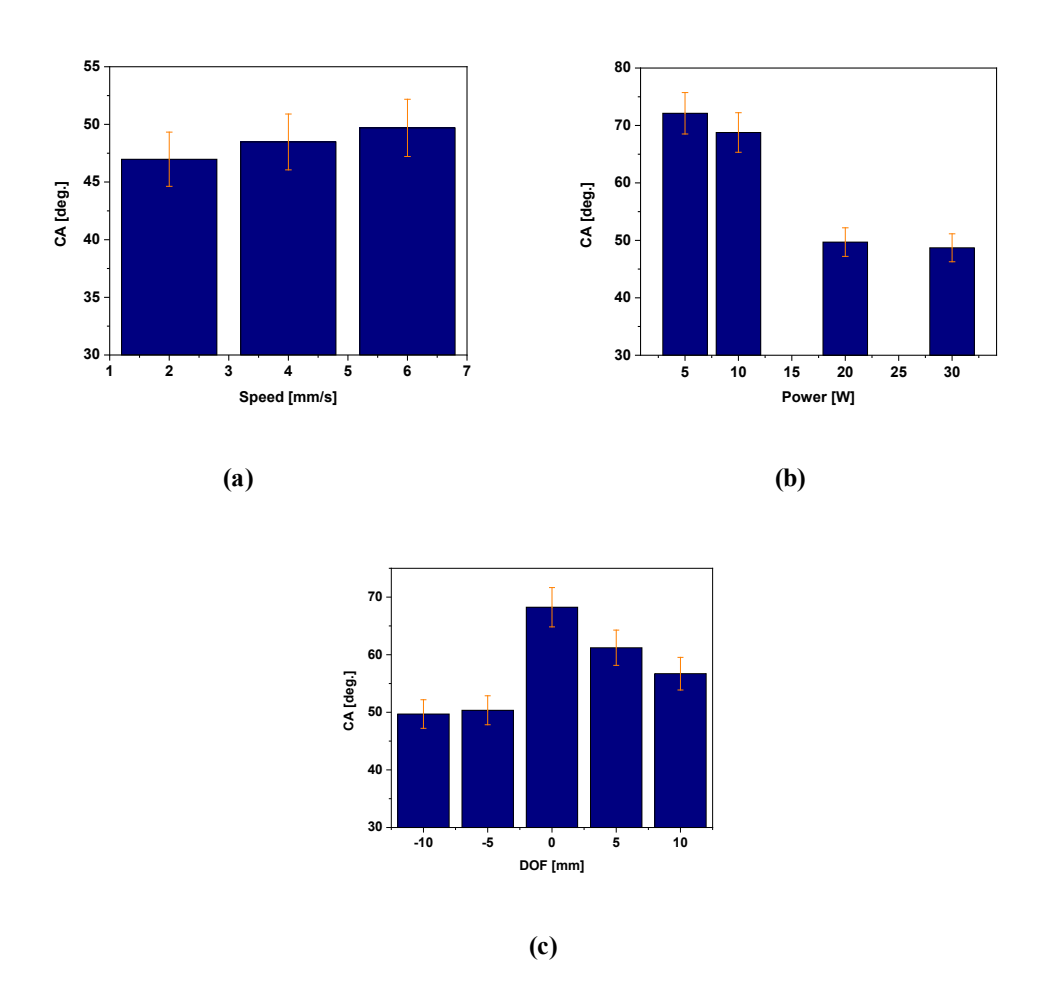


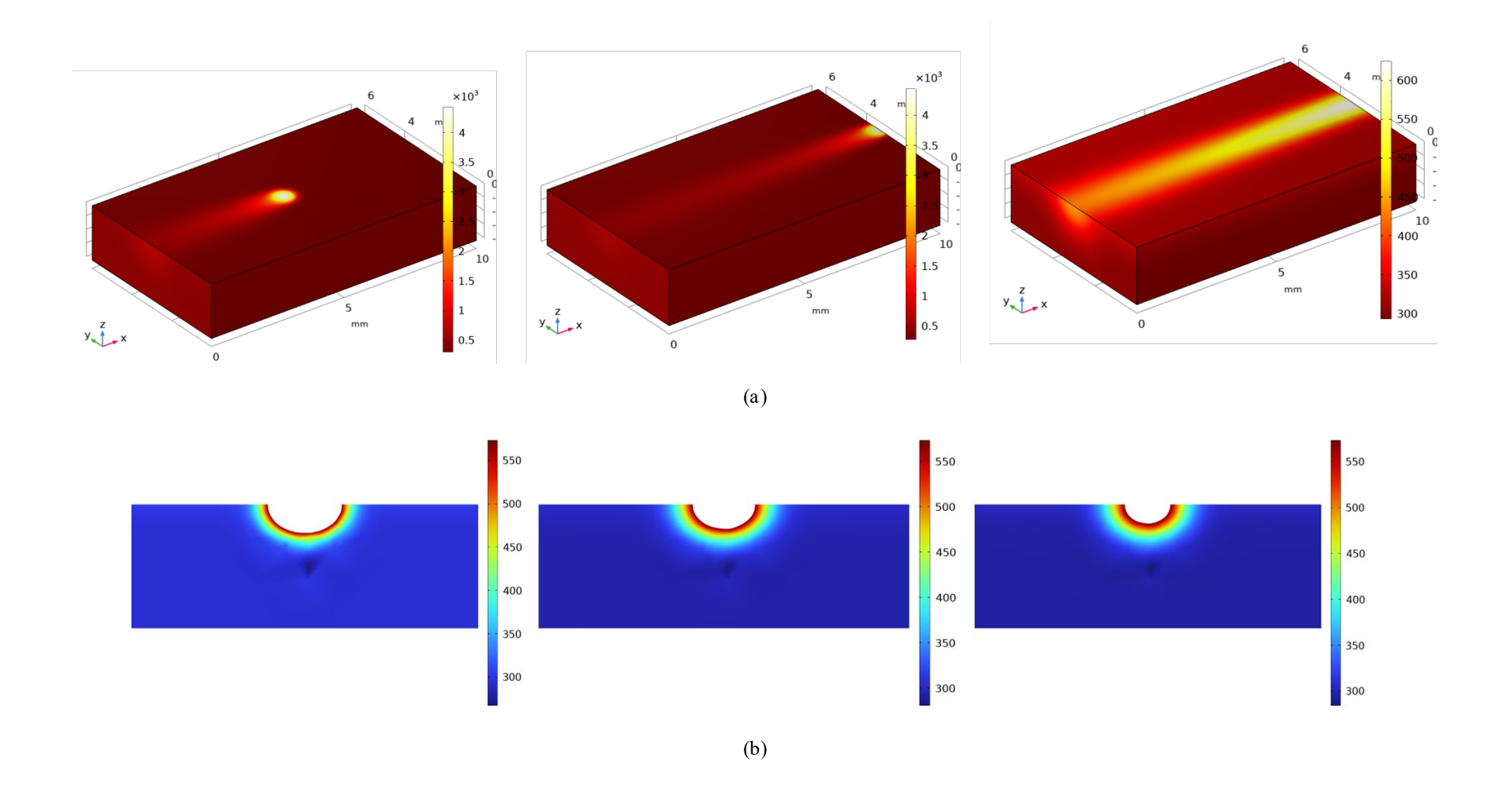
Figure 11: Contact angle change as a function of (a) laser scanning speed, (b) laser power and (c) focus position.

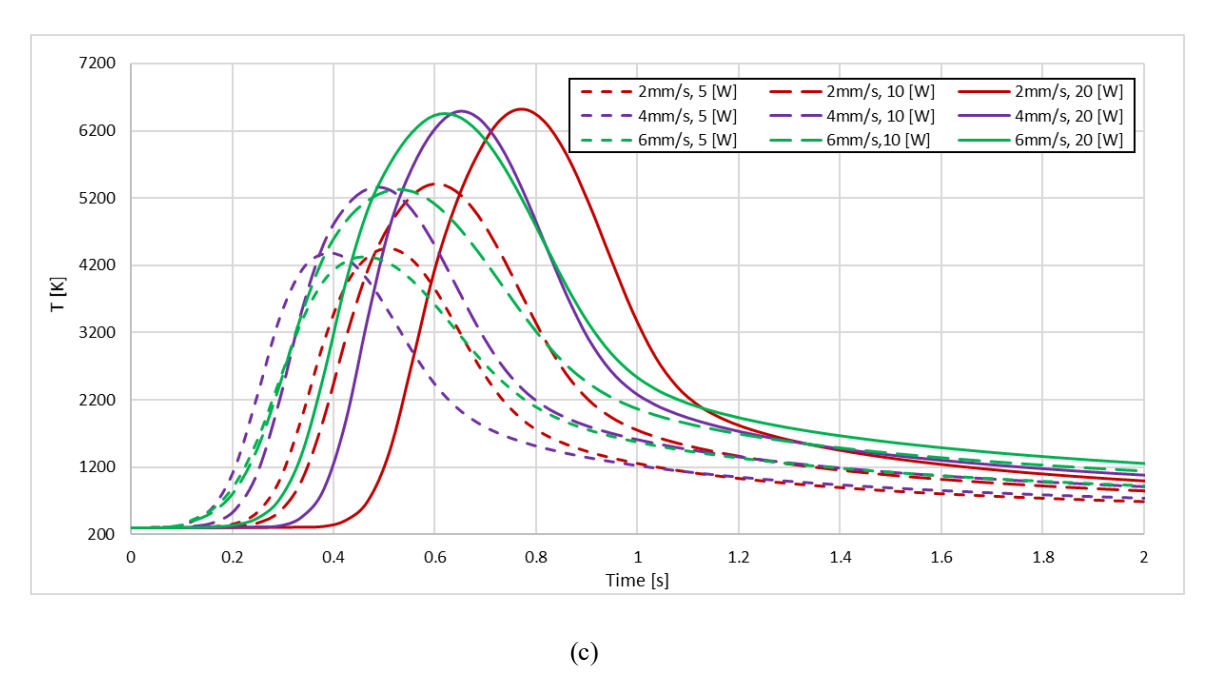
4.2. Thermal Modeling Results

Figure 12 a, b, c and d show the temperature profile recorded after 2.5 second of laser machining, crater profile formed after 0.5s, the surface temperature after 2.5s, surface temperature as a function of depth, respectively, using different powers and scanning speeds. The heat source is located on the surface by moving the source from left to right. It can also be seen that the surface temperature increased with increasing the laser power and decreasing the scanning speed. The crater width and depth also increased with increasing the laser power and decreasing the scanning speed. The maximum simulated depth and width is ~ 0.7 mm and 1 mm using 20W and 2 mm/s while the minimum simulated depth and width is ~ 0.15 mm and 0.3 mm using 5W and 6 mm/s (Figure 12b). The statistical results of the surface temperature as a function of laser

power and scanning speed are present by recording the temperature of a point on the surface of PMMA (Figure 12c). The results show that maximum recorded surface temperature is at 20W and 2 mm/s scanning speed which is 6500 K. It can be also seen machining 10 mm line required 1.2s, 2s and 4.5s using 6mm/s, 4mm/s and 2 mm/s scanning speed, respectively. The crater width and depth are simulated by excluding the mesh nodes with temperature exceeded the boiling temperature after 0.5s of laser heating. At face (2) of the modeled geometry, the change of temperature with depth is simulated and recorded after 0.5s of machining is shown in Figure 12d. It is clear that the temperature is inversely proportional with depth as it decreased with depth.

Due to high absorption of PMMA (95%) to the CO₂ laser beam, the photo-thermal ablation process is the dominant mechanism of CO₂ laser processing of PMMA. The process is starting by absorption of laser radiation followed by heating, melting and vaporization of material without leaving heat effects and melted zones. It was shown that the crater profile was Gaussian due to lambert law and this profile tend to be V shape with working in focus area and U shape by processing out of focus. This is due to higher power density and smaller spot area in focused area compared to out of focused area. The increase and decrease of the crater width and depth is attributed to the increase or decrease actual laser beam diameter. The scanning speed of CO₂ laser machining defines the exposure time. The less the scanning speed, the higher exposure time, the more heat is applied to the surface. Thus, increasing of crater depth and width is resulted due to high absorption of laser radiation power. Increasing the width and depth of microchannel is noticed with increasing the number of passes which is attributed to increase the power deposition. However, the rate of material removal is lower of second pass compared with first pass as after first pass, the distance between the laser and the target is changed due to material removal which changes the laser intensity of penetration and increase the scattering effect (Konari et al. 2021; Roy et al. 2011).





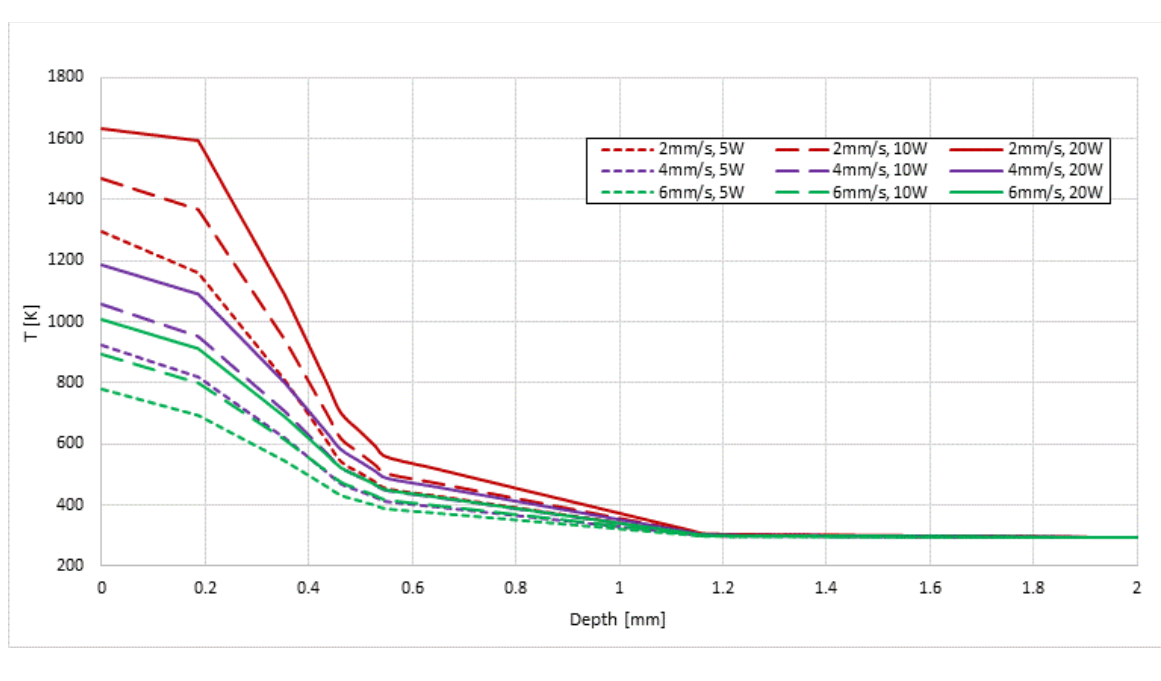


Figure 12: (a) Thermal distribution after one 2.5 seconds, (b) crater profile formed after 0.5s (c) statistical recorded surface temperature, (d) temperature as a function of depth.

(d)

4.3. MFD Design and Characterization

In this work, different design of MFD were implemented and characterized. First of all, the effect of angle has been considered as shown in Figure 13. The results proved that there was no much difference in mixing time by changing the angle from 30° to 90°, as

the recorded time increased slightly from 5 (30°) second to 6 seconds (90°). However, the mixing efficiency using 90° was better than using 30° which was noticed from liquid color change. Also, using 90°, thermal effects on the area around the machined channel and blockages were reduced. Therefore, 90° was chosen to implement the final designs of MFD.

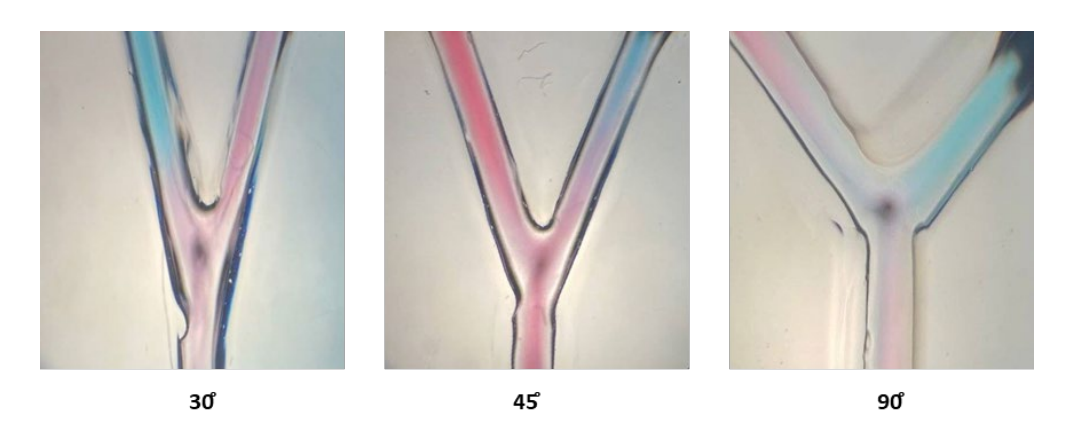


Figure 13: Effect of angle on mixing of liquid.

Figure 14 illustrates the various designs that were developed for the microchannels, including square, zigzag, straight, and others using (20 W laser power, -10 mm focus position, 6 mm/s scanning speed, 5 times processing) laser parameters. Each channel's ability to pass liquid was tested, and the best one was identified. The best outcome was attained in straight and square design (shown in Figure 14A and E) as the liquid flowed through each without any problems (see Figure 6s d in the appendix). However, blockage that stops the liquid from passing after it has been mixed was noted in the other designs (see Figures 6s a-c in the appendix). The heat effect or mechanical causes could be to blame for this. Moreover, the limitation of laser processing parameters (the maximum scanning speed (6mm/s) and minimum spot size 0.5 μm) contributed to some technical problems of blockages and high roughness and thermal effects which causes obstruction to the flow of fluid.

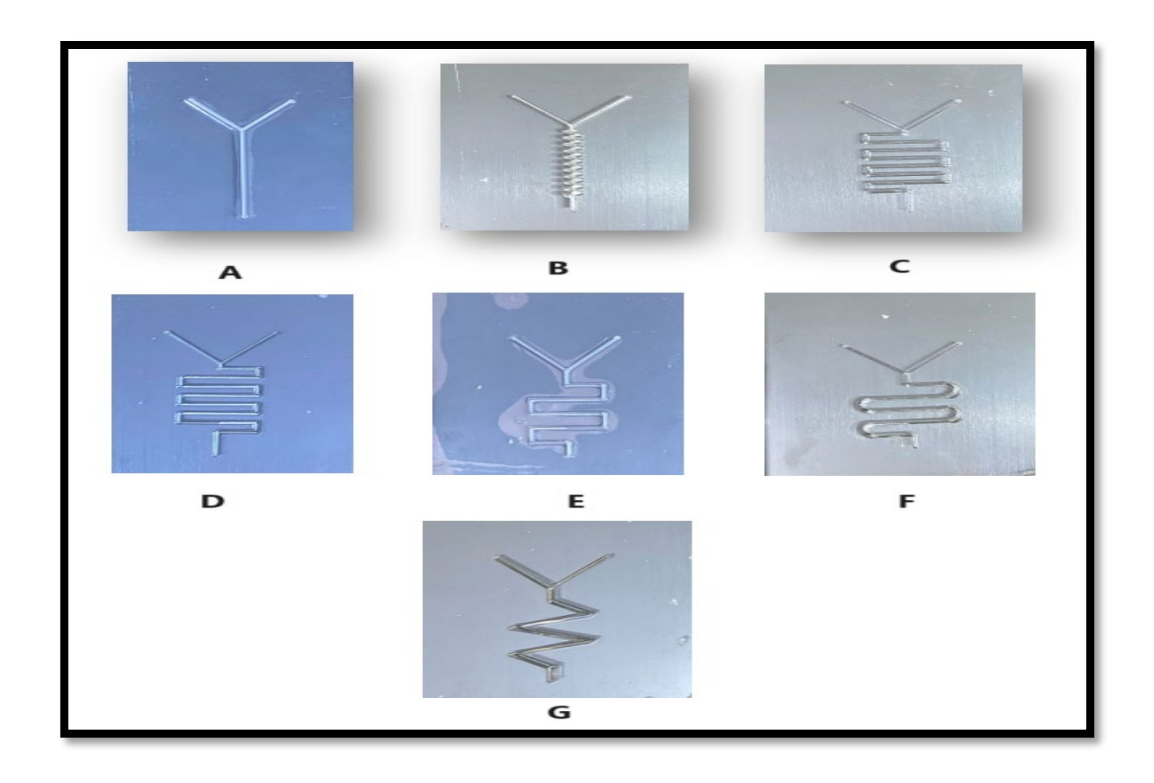


Figure 14: Some designs for microchannels.

4.4. Computational Modeling Results

As the straight and squared channel performed the best fluid flow experimentally, the computational model was carried out to analyze the effect of channel width, length, fluid speed, entry length, angel of incident and channel shape on the concentration change and mixing efficiency (Figures 15-18 and Table 5). By comparing the results presenting in table 5 and Figure 15, it can be seen that changing the channel length from 10mm to 40 mm, the mixing efficiency was increased from 88% to 93.7%. Regarding the channel width, the results showed that decreasing the channel width presented high mixing efficiency to 99.8%. Entry length, on the other hand, also affected the mixing efficiency as it increased from 88% to 94% by changing the entry length from 1 mm to 5 mm. Decreasing the speed of fluid flow (10⁻² m/s to 10⁻⁴ m/s) resulted in increasing the mixing efficiency to around 99%, while changing the liquid diffusivity from 10⁻¹¹ to 10⁻⁸, the mixing efficiency increased from 88% to 96.8%.

Figure 16 shows the velocity magnitude and pressure profile using 10 cm channel length and 30° entry angle. It is clear the pressure at its maximum value when the two fluids enter. However, the pressure drop enhances and reached its maximum value when the mixed fluid leaves the channel. The pressure drop enhances further as the channel's

length increases and the width decreases. The results proved that changing the entry length, angle and diffusivity did not affect the pressure drop performance.

Table 5: Mixing efficiency using different parameters.

Parameter	Magnitude	Mixing Efficiency %
Toronto for all	10	88.4
Length [mm]	40	93.7
	0.1	99.8
Width [mm]	0.5	88.4
	1	88.4
Entry Length [mm]	5	96
A - 1 - 61 - 11 - 4 11 - 1	30	88.4
Angle of incident [deg.]	90	96.9
V1-2/-1/1	0.1	99.1
Velocity [mm/s]	10	88.4
Diffusivity [m2/s]	1.00E-08	96.8
Diffusivity [m²/s]	1.00E-11	88
Squared design	-	99.9

Table 6 compares the simulated maximum mixing efficiency of this work comparing with some previous published work which proved that the micromixer geometer and properties affect the mixing efficiency.

Table 6: Maximum mixing efficiency.

Description	Simulated maximum mixing efficiency %	Ref.
3D model in which different parameters have been characterized such as length, inlet velocity and diffusivity	99.9	(Farahinia and Zhang 2020)
2D model, square channel, different flow rates have been characterize	95.9	(Arockiam et al. 2021)
2D model, Zigzag with semicircular structure	99	(López et al. 2021)
This work	99.9	-

Concentration distribution, on the other hand gives an information about the mixing phenomenon inside the channel. Figure 17 gives information about the mixing distribution using different lengths, widths, angles, entry lengths, and diffusivity. It can be seen that the channel length, width, entry length, fluid speed and diffusivity are highly affecting the concentration change which interns affecting the mixing efficiency.

However, the results show that changing the entry angle did not perform a high effect on the concentration variation which means that any angle can be used for MFD manufacturing with little effect on mixing efficiency. The results agree with other researchers (Farahinia and Zhang 2020), (Bonament et al. 2022).

Figure 18 show how the channel shape plays a major role; squared channel affects the pressure drop to increase and affects the concentration change to record low values compared to straight channel even when the length of channel increased to 40 mm which in turns affects the mixing efficiency and recorded the highest mixing efficiency, reaching 99.9.

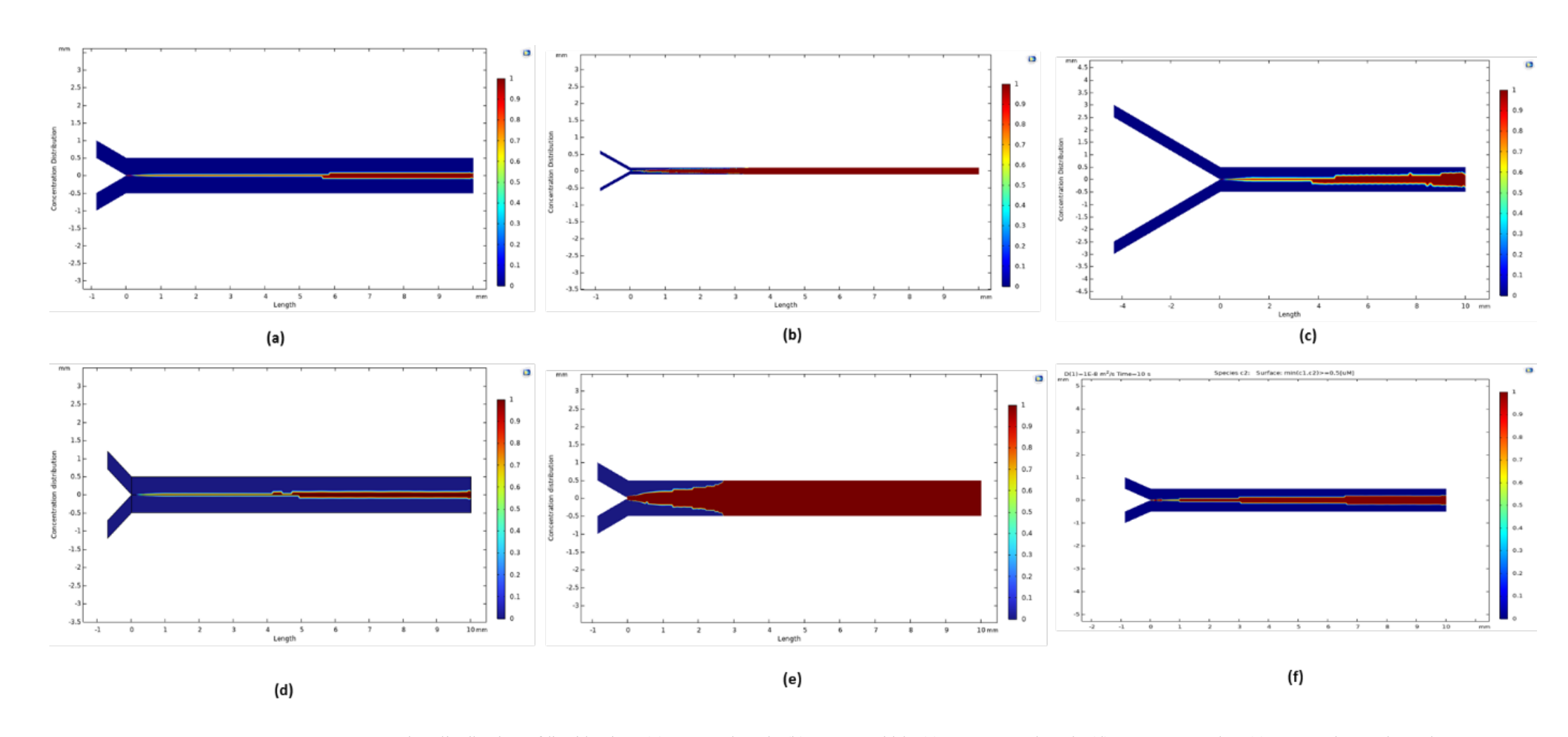


Figure 15: Concertation distribution of liquid using: (a), 10mm length, (b) 0.1mm width, (c) 5mm entry length, (d) 90° entry angles, (e) 0.1 mm/s speeds, and (f) 1.00E-08 diffusivities.

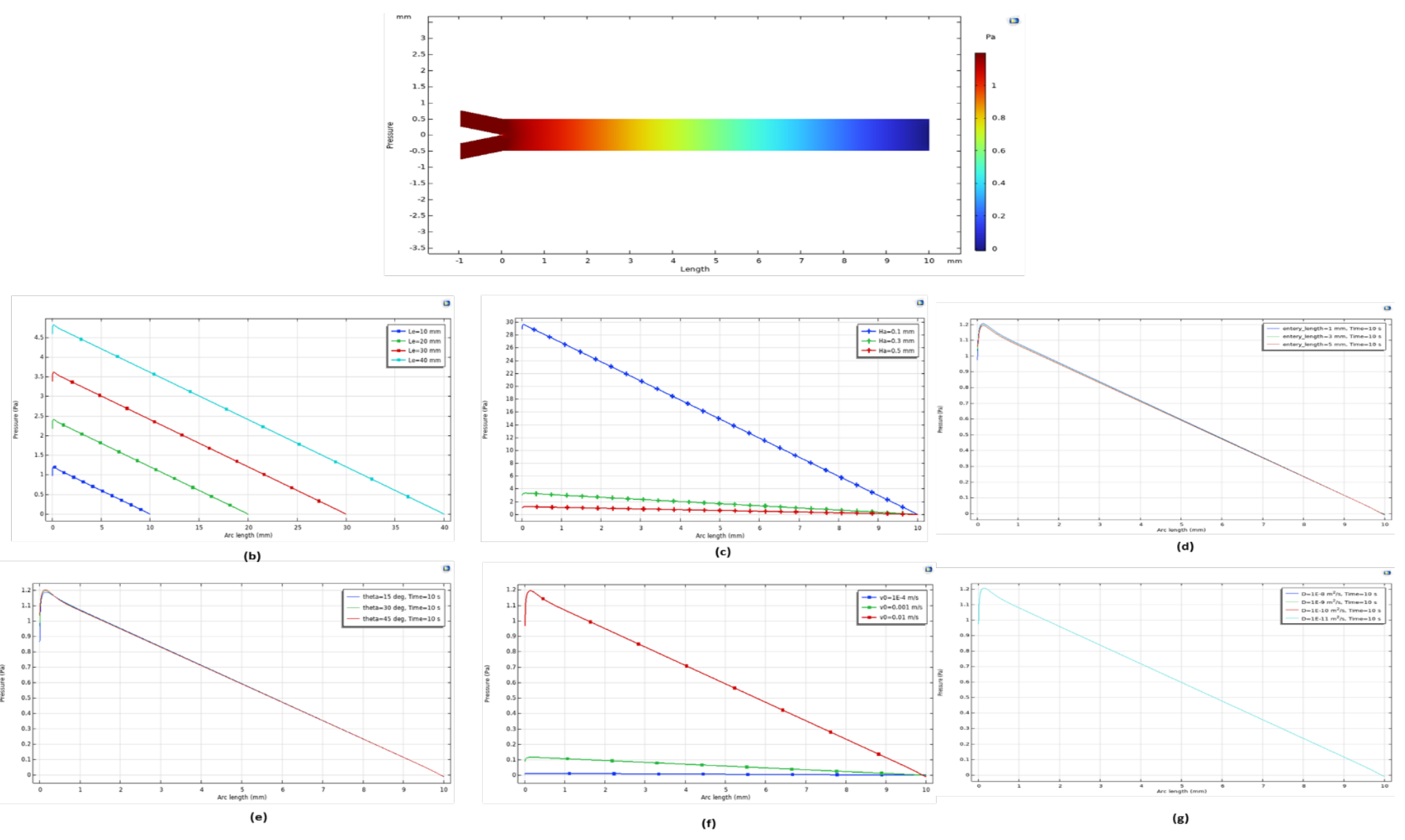


Figure 16: (a) pressure drop using 0.1 m/s, (b) pressure variation using different lengths, (c) pressure variation using different widths, (d) pressure variation using different entry lengths, (e) pressure variation using different entry angle, (f) pressure variation using different speed and (g) pressure variation using different diffusivity.

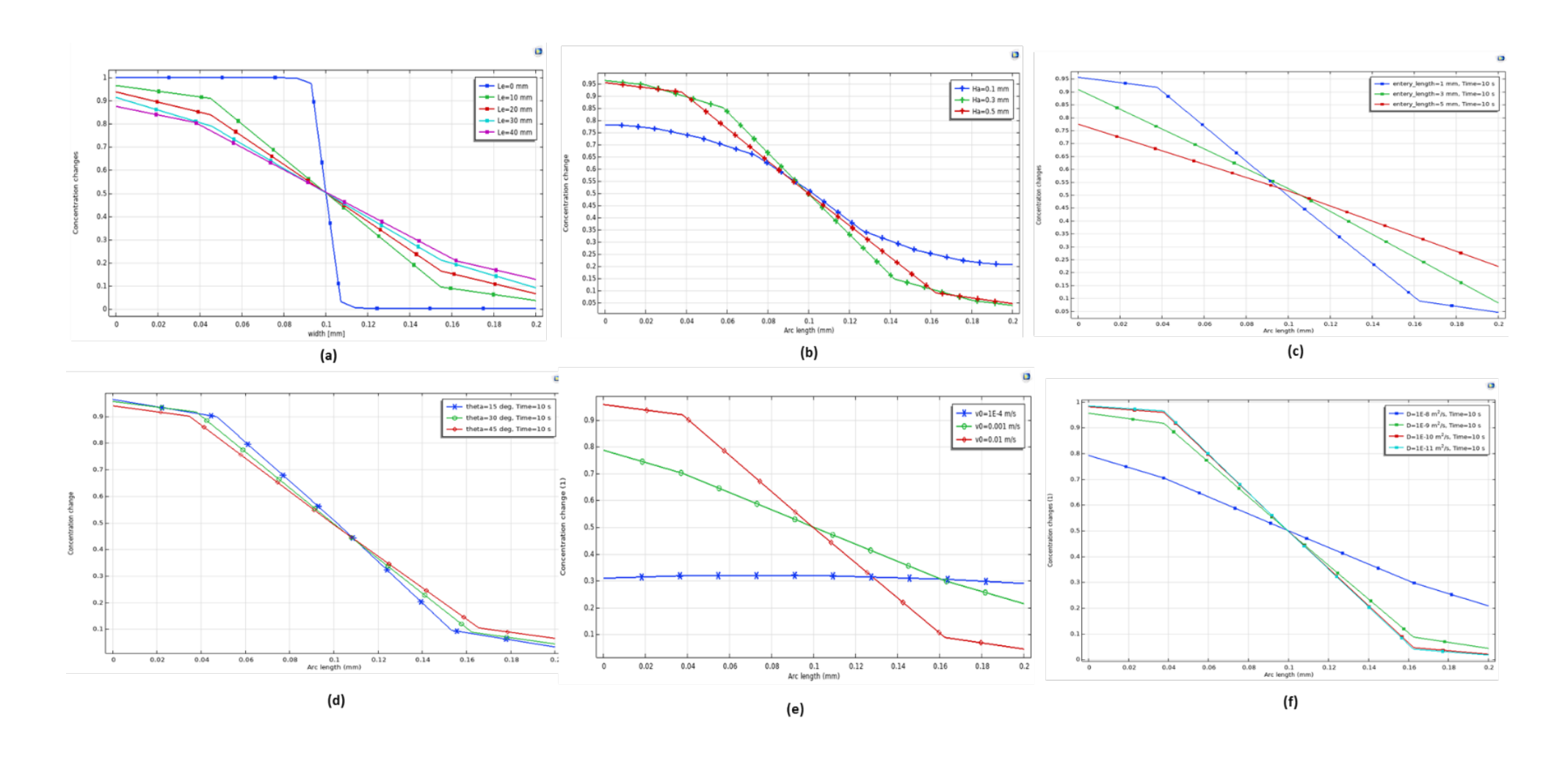


Figure 17: Concertation change of liquid using: (a) different length of channel, (b) different width of channel, (c) different entry length, (d) different entry angles, (e) different speeds, and (f) different diffusivities.

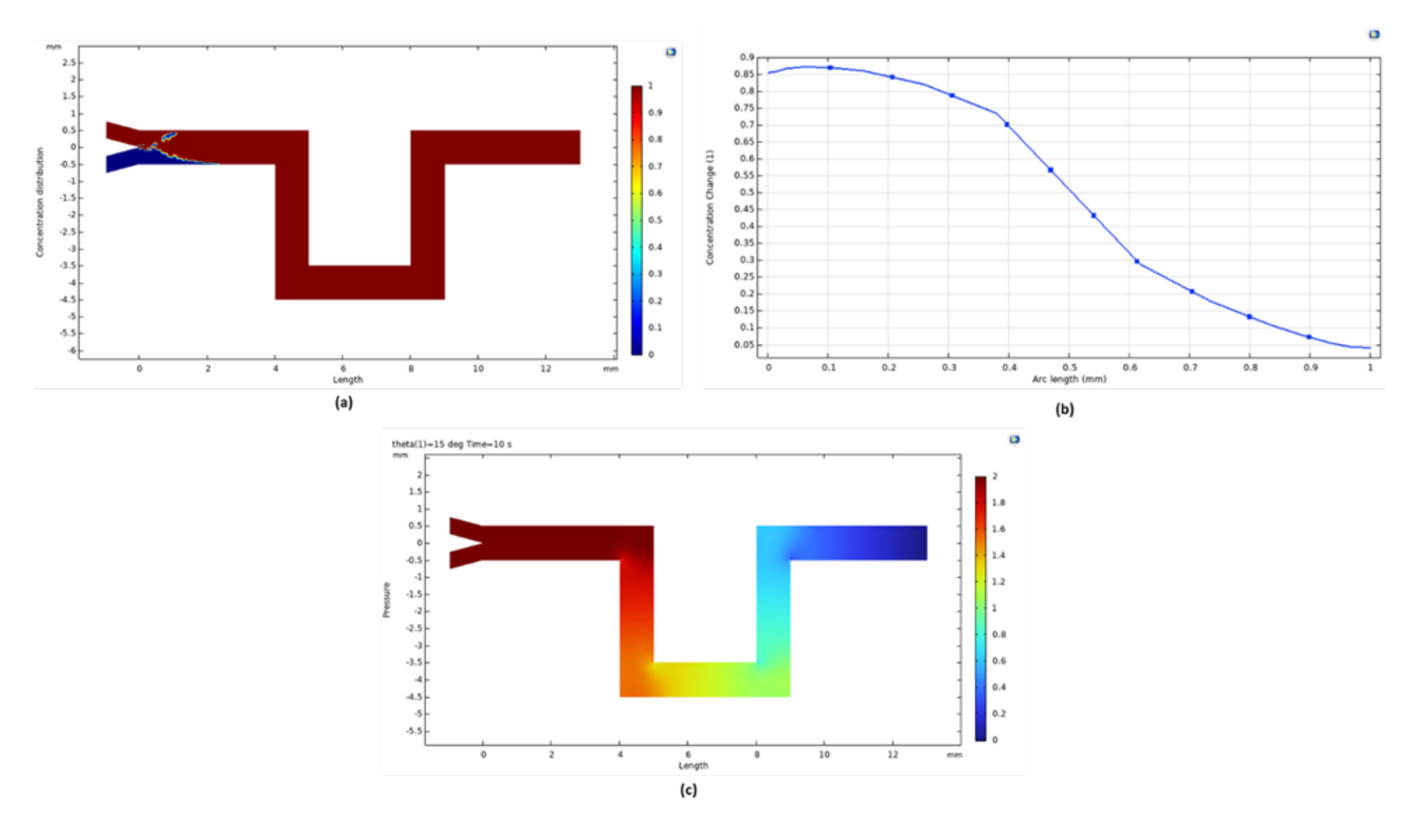


Figure 18: (a) Concertation distribution, (b) concentration change, and (c) pressure drop using squared MFD.

5. Conclusions

In this work, the effect of CO₂ laser processing parameters on micromachining of PMMA polymer was analyzed. The microchannel width, depth and aspect ratio was found to be directly proportional with laser power and number of passes while they inversely proportional with speed due to higher deposition of laser energy and interaction time. V-shaped microchannel was achieved by machining in the focus position while U-shaped microchannel was fabricated on the out of focus region. The results showed that the microchannel depth was increased by 15 times by rising the laser power by only 6 times, while increasing the scanning speed by 3 times, the measured depth was decreased only by 60%. Moreover, depending on the focus position, 0.7mm-0.9mm was the highest recorded width at 30W, 2 mm/s, while less than 0.2 mm was the recorded as the minimum width at 5W, 6 mm/s. Thermal modeling was conducted to simulate the effect of laser parameters on the surface temperature. The surface temperature and microchannel width and depth increased with increasing the laser power and decreasing the scanning speed and the temperature was inversely proportional with depth. Y-micromixer MFD was fabricated on PMMA polymer material using CO₂ laser and the best mixing 96.9% was achieved using 90° inlet angle. The heat accumulation may become an issue when systems with limited travel speed are used and that might affect the performance of MFD and causes the blockage of the channels. Using a laser machine incorporating with highspeed galvo might enhance reduce the heat effects and enhance the MFD performance. Additionally, the laser beam used in this study is continuous beam that cannot be modulated in comparison to the pulsed laser systems that offer full control of the energy input used for specific application. Moreover, a numerical analysis of mixing performance of Y-micromixer with different geometry, cross sections, inlet angles, inlet velocities and diffusion coefficient was conducted using 2D computational fluid dynamics simulation. The mixing efficiency increased with increasing the channel length, width, entry length, entry angle, fluid velocity and diffusivity. Indeed, the geometry design affected the mixing efficiently and the squared geometry performed the highest mixing efficiency 99.9%.

References

Abgrall, P., Gue, A.M.: Lab-on-chip technologies: making a microfluidic network and coupling it into a complete microsystem—a review. Journal of micromechanics and microengineering. 17, R15 (2007)

Aralekallu, S., Boddula, R., Singh, V.: Development of glass-based microfluidic devices: A review on its fabrication and biologic applications. Mater Des. 111517 (2022)

Arockiam, S., Cheng, Y.H., Armenante, P.M., Basuray, S.: Experimental determination and computational prediction of the mixing efficiency of a simple, continuous, serpentine-channel microdevice. Chemical Engineering Research and Design. 167, 303–317 (2021)

Baccar, N., Kieffer, R., Charcosset, C.: Characterization of mixing in a hollow fiber membrane contactor by the iodide–iodate method: Numerical simulations and experiments. Chemical Engineering Journal. 148, 517–524 (2009)

Becker, H., Gärtner, C.: Polymer microfabrication technologies for microfluidic systems. Anal Bioanal Chem. 390, 89–111 (2008)

Becker, H., Locascio, L.E.: Polymer microfluidic devices. Talanta. 56, 267–287 (2002)

Bonament, A., Prel, A., Sallese, J.-M., Lallement, C., Madec, M.: Analytic modelling of passive microfluidic mixers. Mathematical Biosciences and Engineering. 19, 3892–3908 (2022)

Cai, J., Jiang, J., Gao, F., Jia, G., Zhuang, J., Tang, G., Fan, Y.: Rapid prototyping of cyclic olefin copolymer based microfluidic system with CO 2 laser ablation. Microsystem Technologies. 23, 5063–5069 (2017)

Chen, J.M., Horng, T.-L., Tan, W.Y.: Analysis and measurements of mixing in pressure-driven microchannel flow. Microfluid Nanofluidics. 2, 455–469 (2006)

Conlisk, A.T.: Essentials of micro-and nanofluidics: with applications to the biological and chemical sciences. Cambridge University Press (2012)

Farahinia, A., Zhang, W.J.: Numerical analysis of a microfluidic mixer and the effects of different cross-sections and various input angles on its mixing performance. Journal of the Brazilian Society of Mechanical Sciences and Engineering. 42, 1–18 (2020)

Gucluer, S., Guler, O.: A Low-Cost Laser-Prototyped Microfluidic Device for Separating Cells and Bacteria. Applied Sciences. 13, 7938 (2023)

Heckele, M., Bacher, W., Müller, K.D.: Hot embossing-the molding technique for plastic microstructures. Microsystem technologies. 4, 122–124 (1998)

Iliescu, C., Taylor, H., Avram, M., Miao, J., Franssila, S.: A practical guide for the fabrication of microfluidic devices using glass and silicon. Biomicrofluidics. 6, (2012)

Kexin Gao, Jingji Liu, Yiqiang Fan, Yajun Zhang: Ultra-low-cost fabrication of polymer-based microfluidic devices with diode laser ablation. (2019)

Khan Malek, C.G.: Laser processing for bio-microfluidics applications (part I). Anal Bioanal Chem. 385, 1351–1361 (2006)

Konari, P.R., Clayton, Y.-D., Vaughan, M.B., Khandaker, M., Hossan, M.R.: Experimental analysis of laser micromachining of microchannels in common microfluidic substrates. Micromachines (Basel). 12, 138 (2021)

Li, K., Xu, G., Huang, X., Xie, Z., Gong, F.: Manufacturing of micro-lens array using contactless micro-embossing with an EDM-mold. Applied Sciences. 9, 85 (2018)

Lippert, T.: Laser application of polymers. Polymers and Light. 51–246 (2004)

López, R.R., Sánchez, L.-M., Alazzam, A., Burnier, J. V, Stiharu, I., Nerguizian, V.: Numerical and experimental validation of mixing efficiency in periodic disturbance mixers. Micromachines (Basel). 12, 1102 (2021)

LoTurco, S., Osellame, R., Ramponi, R., Vishnubhatla, K.C.: Hybrid chemical etching of femtosecond laser irradiated structures for engineered microfluidic devices. Journal of Micromechanics and Microengineering. 23, 085002 (2013)

Mahdee Samae · Pawarit Ritmetee · Somyot Chirasatitsin · Sanja Kojić · Tijana Kojić · Jovana Jevremov · Goran Stojanović · Hani Al Salami: Precise Manufacturing and Performance Validation of Paper-Based Passive Microfuidic Micromixers. (2019)

Malek, C.G.K.: Laser processing for bio-microfluidics applications (part 1). Anal.Bioanal.Chem. 385, 1351–1361 (2006)

Matellan, C., del Río Hernández, A.E.: Cost-effective rapid prototyping and assembly of poly (methyl methacrylate) microfluidic devices. Sci Rep. 8, 6971 (2018)

McDonald, J.C., Duffy, D.C., Anderson, J.R., Chiu, D.T., Wu, H., Schueller, O.J.A., Whitesides, G.M.: Fabrication of microfluidic systems in poly (dimethylsiloxane). ELECTROPHORESIS: An International Journal. 21, 27–40 (2000)

Prakash, S., Kumar, S.: Fabrication of microchannels on transparent PMMA using CO 2 Laser (10.6 μ m) for microfluidic applications: An experimental investigation. International Journal of Precision Engineering and Manufacturing. 16, 361–366 (2015)

Prakash, S., Kumar, S.: CO2 laser microchanneling process: effects of compound parameters and pulse overlapping. In: IOP Conference Series: Materials Science and Engineering. p. 012018. IOP Publishing (2016)

Prakash, S., Kumar, S.: Fabrication of rectangular cross-sectional microchannels on PMMA with a CO2 laser and underwater fabricated copper mask. Opt Laser Technol. 94, 180–192 (2017)

Prakash, S., Kumar, S.: Determining the suitable CO2 laser based technique for microchannel fabrication on PMMA. Opt Laser Technol. 139, 107017 (2021)

Rajab, F.H., Al-Hamd, R.K.S.: Surface Characterization of Laser Processing of Ti6Al4V in Air and Underwater. Journal of Russian Laser Research. 1–11 (2023)

Rajab, F.H., Al-Jumaily, A.K., AS, T.T., Stanescu, S.L., AlShaer, A.W., Li, L., Al-Hamd, R.K.S.: A comparison of characteristics of periodic surface micro/nano structures generated via single laser beam direct writing and particle lens array parallel beam processing. Journal of Microand Nano-Manufacturing. 9, 021007 (2021)(a)

Rajab, F.H., AS, T.T., Al-Jumaily, A.K., AlShaer, A.W., Li, L., Whitehead, K.A.: The influence of picosecond laser generated periodic structures on bacterial behaviour. Appl Surf Sci. 540, 148292 (2021)(b)

Rajab, F.H., Liu, Z., Li, L.: Production of stable superhydrophilic surfaces on 316L steel by simultaneous laser texturing and SiO2 deposition. Appl Surf Sci. 427, 1135–1145 (2018)

Rajab, F.H., Whitehead, D., Liu, Z., Li, L.: Characteristics of hierarchical micro/nano surface structure formation generated by picosecond laser processing in water and air. Applied Physics B. 123, 1–12 (2017)

Ravi-Kumar, S., Lies, B., Zhang, X., Lyu, H., Qin, H.: Laser ablation of polymers: A review. Polym Int. 68, 1391–1401 (2019)

Roy, S., Yue, C.Y., Venkatraman, S.S., Ma, L.L.: Low-temperature (below Tg) thermal bonding of COC microfluidic devices using UV photografted HEMA-modified substrates: high strength, stable hydrophilic, biocompatible surfaces. J Mater Chem. 21, 15031–15040 (2011)

Sanja P. Kojic, G.M.S. and V.R.,: Novel Cost-Effective Microfluidic Chip Based on Hybrid Fabrication and Its Comprehensive Characterization. (2019)

Sungil Kim, J.K., Y.-H.J., J.C., Chiwan K.,: Bonding Strength of a Glass Microfluidic Device Fabricated by Femtosecond Laser Micromachining and Direct Welding. (2018)

Ting-Fu Hong, Wei-Jhong Ju, Ming-Chang Wu, Chang-Hsien Tai, Chien-Hsiung Tsai, Lung-Ming Fu: Rapid prototyping of PMMA microfluidic chips utilizing a CO2 laser. (2010)

Vannoy, C.H., Tavares, A.J., Noor, M.O., Uddayasankar, U., Krull, U.J.: Biosensing with quantum dots: a microfluidic approach. Sensors. 11, 9732–9763 (2011)

Verpoorte, E.: Microfluidic chips for clinical and forensic analysis. Electrophoresis. 23, 677–712 (2002)

Verpoorte, E., De Rooij, N.F.: Microfluidics meets MEMS. Proceedings of the IEEE. 91, 930–953 (2003)

Vora, H.D., Santhanakrishnan, S., Harimkar, S.P., Boetcher, S.K.S., Dahotre, N.B.: One-dimensional multipulse laser machining of structural alumina: evolution of surface topography. The International Journal of Advanced Manufacturing Technology. 68, 69–83 (2013)

Wlodarczyk, K.L., Hand, D.P., Maroto-Valer, M.M.: Maskless, rapid manufacturing of glass microfluidic devices using a picosecond pulsed laser. Sci Rep. 9, 20215 (2019)

Yiqiang Fan Huawei Li Ying Yi Ian G. Foulds: Laser micromachined wax-covered plastic paper as both sputter deposition shadow masks and deep-ultraviolet patterning masks for polymethylmethacrylate-based microfluidic systems. (2013)

Yundong Ren, Subhrodeep Ray, Yuxiang Liu: Reconfgurable Acrylic-tape Hybrid Microfuidics. (2019)